Received: 1 July 2023 | Accepted: 22 August 2023

DOI: 10.1002/pamm.202300215

RESEARCH ARTICLE

Simulation of precipitate hardening in ferroelectric material

Matthias Bohnen | **Ralf Müller**

Institute for Mechanics, Technical University of Darmstadt, Darmstadt, Germany

Correspondence
Matthias Bohnen, Institute for Mechanics, Technical University of Darmstadt, Darmstadt, Germany.
Email: matthias.bohnen@tu-darmstadt.de

Funding information
DFG, Grant/Award Number: 528293120

Abstract

Precipitate hardening is introduced as a mechanism to tune the reaction of ferroelectric materials to the application of an external electric field. For this purpose, a phase field model for polarization in ferroelectric material is presented in this paper. Different materials with and without precipitates are simulated and the respective hysteresis curves for charge and macroscopic strain are derived. The results show a reduction of the hysteresis curves if precipitates are present in the material, which confirms the experimental observation of recent material studies.

1 | INTRODUCTION

Precipitate hardening is well established in metals and ceramics. This treatment aims at modifying mechanical properties of the material such as stiffness or crack resistance [1, 2]. Recent studies have shown that this technique can also be applied to ferroelectric materials, where it is an alternative to doping by foreign atoms to modify the electromechanical properties of the material [3]. Precipitates or doping effectively reduces domain wall mobility and heat dissipation, which results in narrower hysteresis loops of polarization versus applied electric field. Thus, the mechanical quality factor can be enhanced [4]. However, determining the optimal shape and size of the precipitates remains an open question. In [4], for example, the observed precipitates appear to be plate like, with an elongated elliptical cross section.

In this work, we present a phase field model for the polarization field in ferroelectric materials. We simulate the movement of domain walls in homogeneous and different heterogeneous materials, for the application of an external electric potential. The charge on the boundary and the macroscopic strain are derived from the solution to display the characteristic hysteresis and butterfly hysteresis loops of the underlying material. As these hysteresis loops are an indicator for loss, the goal is to observe a narrowing of the hysteresis if precipitates are introduced to the material.

2 | PHASE FIELD MODEL FOR POLARIZATION

For the two-dimensional approach in this work, we consider the x_1, x_3-plane of a cartesian coordinate system and assume small deformations. With the displacement vector $\vec{u} = (u_1, u_3)^T$, the mechanical strain is defined as the symmetric displacement gradient

$$\boldsymbol{\varepsilon} = \frac{1}{2}\left(\operatorname{grad} \vec{u} + \operatorname{grad}^T \vec{u}\right). \tag{1}$$

In all formulas Voigt notation will be used consistently for the x_1, x_3-plane, denoted by an underline, with

$$\underline{\boldsymbol{\varepsilon}} = (\varepsilon_{11},\ \varepsilon_{33},\ 2\varepsilon_{13})^T. \tag{2}$$

The electric field is defined as the gradient of the electric potential φ via

$$\vec{E} = -\nabla\varphi. \tag{3}$$

The phase field model used for the simulation is based on [5]. Here, the phase field potential of the system comprises three parts: An electric enthalpy H^{ent}, a phase separation potential H^{sep}, and an interface energy H^{int}.

$$H = H^{\text{ent}}(\boldsymbol{\varepsilon}, \vec{E}, \vec{P}) + H^{\text{sep}}(\vec{P}) + H^{\text{int}}(\nabla\vec{P}), \tag{4}$$

with

$$H^{\text{ent}} = \frac{1}{2}(\boldsymbol{\varepsilon} - \boldsymbol{\varepsilon}_0)\cdot\mathbb{C}(\boldsymbol{\varepsilon} - \boldsymbol{\varepsilon}_0) - (\boldsymbol{\varepsilon} - \boldsymbol{\varepsilon}_0)\cdot\mathbb{e}^T\vec{E} - \frac{1}{2}\vec{E}\cdot\mathbb{d}\vec{E} - \vec{P}\cdot\vec{E}, \tag{5a}$$

$$H^{\text{sep}} = \kappa_s\frac{\gamma}{l}\psi(\vec{P}), \tag{5b}$$

$$H^{\text{int}} = \frac{1}{2}\kappa_i\frac{\gamma l}{P_0^2}||\nabla\vec{P}||^2. \tag{5c}$$

The constants l and γ represent the interface width and energy density. κ_s and κ_i are two calibration constants. The stiffness matrix $\mathbb{C}$ is assumed orthotropic and the dielectric matrix $\mathbb{d}$ isotropic. Both are locally defined for the simulation of heterogeneous material.

The constitutive equations for the Cauchy stress can be derived from the electric enthalpy (4–5c) by

$$\boldsymbol{\sigma} = \frac{\partial H}{\partial\boldsymbol{\varepsilon}} = \mathbb{C}(\boldsymbol{\varepsilon} - \boldsymbol{\varepsilon}_0) - \mathbb{e}^T\vec{E}, \tag{6}$$

and for the dielectric displacement as

$$\vec{D} = -\frac{\partial H}{\partial\boldsymbol{E}} = \mathbb{e}(\boldsymbol{\varepsilon} - \boldsymbol{\varepsilon}_0) + \mathbb{d}\vec{E} + \vec{P}. \tag{7}$$

With reference to [6], the spontaneous strain is formulated as

$$\boldsymbol{\varepsilon}_0(\vec{P}) = \frac{3}{2}\varepsilon_0\left(\frac{||\vec{P}||}{P_0}\right)^2\left\{\vec{e}\otimes\vec{e} - \frac{1}{3}\mathbb{1}\right\}, \tag{8}$$

with ε_0, the spontaneous strain of the unloaded ferroelectric phase and P_0, the value of the spontaneous polarization of the unloaded phase. The vector $\vec{e} = \vec{P}/||\vec{P}||$ represents the direction of poling.

The inverse piezoelectric effect is assumed to be transversally isotropic [6]:

$$\mathbb{e}_{kij}(\vec{P}) = \left(\frac{||\vec{P}||}{P_0}\right)^{\nu}\left\{\mathrm{e}_{333}e_ie_je_k + \mathrm{e}_{311}(\delta_{ij} - e_ie_j)e_k + \mathrm{e}_{131}\frac{1}{2}\left[(\delta_{ki} - e_ke_i)e_j + (\delta_{kj} - e_ke_j)e_i\right]\right\}, \tag{9}$$

with the locally defined stress coefficients of the inverse piezoelectric effect e_{333}, e_{311}, and e_{131}. We set $\nu = 3$ to ensure the smoothness of H^{ent} at $\vec{P} = \vec{0}$.

Based on [5], the energy landscape of the phase field is described by the fourth-order polynomial ψ as

$$\psi(\vec{P}) = 1 + \frac{a_1}{P_0^2}(P_1^2 + P_2^2) + \frac{a_2}{P_0^4}(P_1^4 + P_2^4) + \frac{a_3}{P_0^4}(P_1^2P_2^2) + \frac{a_4}{P_0^6}(P_1^6 + P_2^6). \tag{10}$$

The order parameter $\vec{P}$ for the spontaneous polarization evolves with time by a Ginzburg–Landau type equation

$$\beta\dot{\vec{P}} = \kappa_i \frac{\gamma l}{P_0^2}\Delta\vec{P} - \kappa_s \frac{\gamma}{l}\frac{\partial\psi}{\partial\vec{P}} - \frac{\partial H^{\text{ent}}}{\partial\vec{P}}, \tag{11}$$

with the mobility constant β.

The stress $\boldsymbol{\sigma}$ and the dielectric displacement $\vec{D}$ satisfy the following balance laws:

$$\operatorname{div}\boldsymbol{\sigma} = \vec{0}, \tag{12a}$$

$$\operatorname{div}\vec{D} = 0. \tag{12b}$$

2.1 | Numerics

The model was implemented using the finite element library of the FEniCS Project [7, 8]. Mixed elements with linear continuous ansatz functions were used to perform the computations. The evolution Equation (11) was discretized with a backward difference scheme.

2.2 | Model parameters

A material set for lead zirconate titanate (PZT-5H) [9] was defined as the matrix material (m) in the simulations. We set

$$\underline{\mathbb{C}}^{\text{m}} = \begin{bmatrix} 13 & 5.0 & 0 \\ 5.0 & 13 & 0 \\ 0 & 0 & 4.0 \end{bmatrix} \cdot 10^{10}\frac{\text{N}}{\text{m}^2}, \tag{13a}$$

$$\underline{\mathbb{d}}^{\text{m}} = \begin{bmatrix} 1.3 & 0 \\ 0 & 1.3 \end{bmatrix} \cdot 10^{-8}\frac{\text{C}}{\text{Vm}}, \tag{13b}$$

$$\text{e}^{\text{m}}_{333} = 23.3\frac{\text{C}}{\text{m}^2},\ \text{e}^{\text{m}}_{311} = -6.5\frac{\text{C}}{\text{m}^2},\ \text{e}^{\text{m}}_{131} = 17.0\frac{\text{C}}{\text{m}^2}. \tag{13c}$$

In the heterogeneous case, the local elastic constants for the precipitates (p) are assumed to be

$$\underline{\mathbb{C}}^{\text{p}} = \frac{1}{10}\underline{\mathbb{C}}^{\text{m}}, \tag{14}$$

and all dielectric and piezoelectric constants as well as the spontaneous polarization and strain are set to zero.

The values for the spontaneous polarization and strain in the matrix domain are estimated to

$$P_0 = 0.32\frac{\text{C}}{\text{m}^2},\ \varepsilon_0 = 0.0057, \tag{15}$$

and the dimensionless parameters of Equation (10) set to

$$a_1 = -1.125,\ a_2 = -0.75,\ a_3 = 3.3,\ a_4 = 0.875. \tag{16}$$

The inverse of the mobility constant for the domain wall motion in PZT-5H is chosen as

$$\beta^{-1} = 0.32 \cdot 10^3\text{A/Vm}, \tag{17}$$

and the calibration constants for the energy landscape

$$\kappa_s = 0.71,\ \kappa_i = 0.35. \tag{18}$$

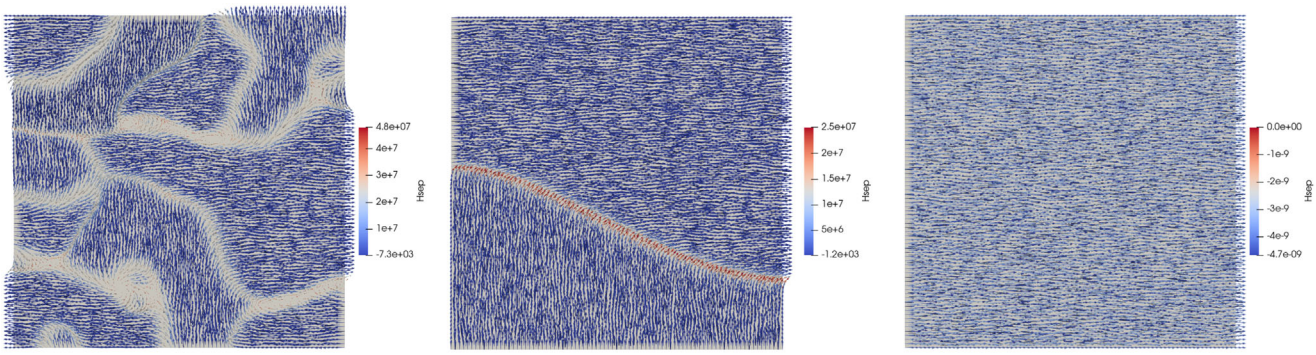

(A) (B) (C)

FIGURE 1 Phase field, colored in phase separation potential, after randomly initialized polarization. (A) Shortly after initialization, (B) metastable 90° domain wall, (C) final configuration.

3 | EQUILIBRIUM IN HOMOGENEOUS MATERIAL

The model is first subjected to the boundary condition of $\varphi = 0$ on the entire boundary. The initial configuration consists of randomly oriented polarization vectors, that then solve into an equilibrium state. This can be seen in Figure 1, where three time steps of the evolution are shown. The color indicates the phase separation potential. Shortly after the initialization, the polarization field organizes in a vortex-like structure, as Figure 1A shows. The vortexes vanish over time and a metastable 90° domain wall is created (Figure 1B). As the domain wall moves downward, the lower domain finally vanishes until a mono-domain is created as the final equilibrium state, displayed in Figure 1C.

4 | SIMULATION OF DOMAIN WALL MOVEMENT

The motion of the domain walls is analyzed in this section by means of a time-dependent boundary condition. First, a 180° domain wall with an initially sharp interface is exposed to the boundary condition $\varphi = 0$ on the upper and the lower boundary, until the phase field is established. This is the point in time t^* at which a sinusoidal boundary condition is activated on the upper boundary with

$$\varphi^* = 1\mathrm{V} \sin\left(\frac{2\pi}{T}(t - t^*)\right), \text{ for } t \geq t^*. \tag{19}$$

Due to the sign change of Equation (19), the domain wall first moves to the right before moving back left, which is then repeated for a second period. As Figure 2 shows, the amplitude is chosen such that the domain wall never reaches the end of the material so it does not dissolve completely.

The charge on a surface ∂V of the body with volume V is given by

$$Q = \int_{\partial V_{\text{bottom}}} \vec{D}\vec{n}\mathrm{ds}, \tag{20}$$

with the outward pointing normal vector $\vec{n}$. In all simulations, we compute the integral over the lower boundary $\partial V_{\text{bottom}}$ of the domain.

The macroscopic strain is computed as the volume average of the strains:

$$\bar{\varepsilon}_{33} = \frac{1}{V}\int_V \varepsilon_{33}\mathrm{dV}. \tag{21}$$

The simulation was performed for three different material distributions. Figure 5A first shows the charge with respect to the applied electric potential for a homogeneous body. The curve displays a hysteresis loop that is the same for both periods of the boundary condition. Figure 5B shows the expected butterfly-like hysteresis for the macroscopic strain of the applied electric potential.

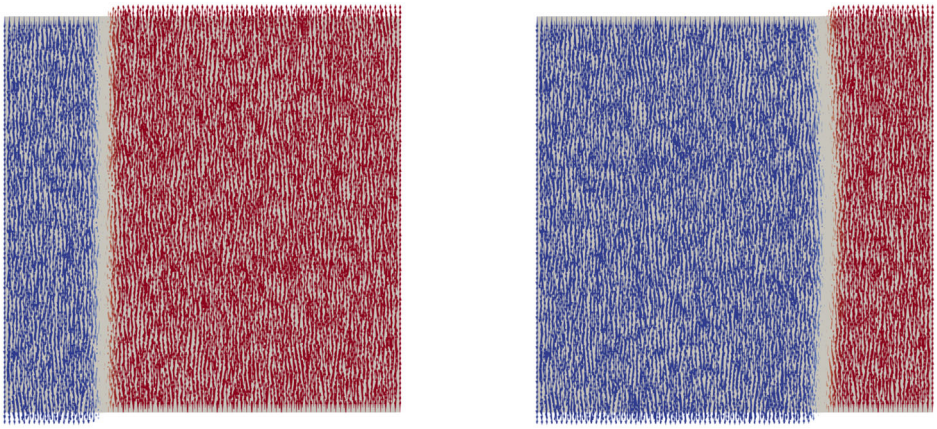

(A) (B)

FIGURE 2 Phase field with 180° domain wall for homogeneous material: (A) initial configuration and (B) at half period time.

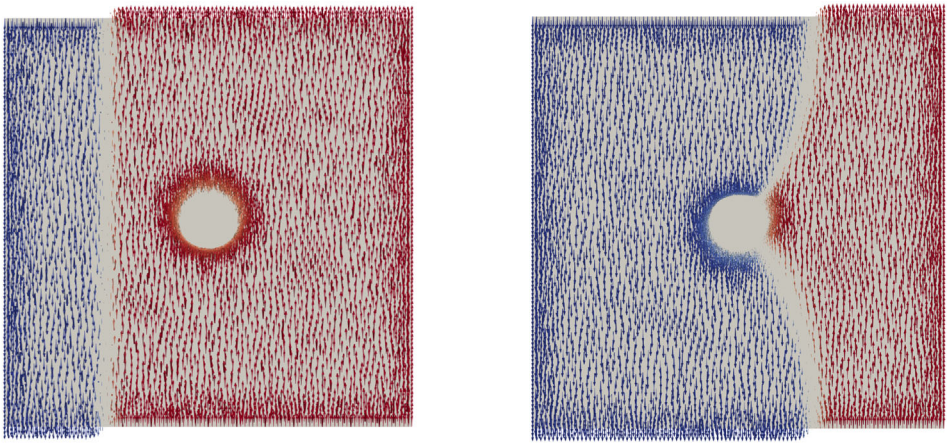

(A) (B)

FIGURE 3 Phase field with 180° domain wall for material with circular inclusion: (A) initial configuration and (B) pinned.

The simulation is then repeated for a heterogeneous material with a circular inclusion. Because of the potential difference between the upper and the lower boundary, the domain wall is first shifted to the right. When it reaches the inclusion in the first period, the domain wall attaches perpendicular to the surface of the inclusion. Throughout the rest of the simulation and all further periods of the cyclic boundary condition, the domain wall remains pinned to the inclusion, as can be seen in Figure 3B. Figure 6 shows the respective charge and strain with respect to the applied potential on the upper boundary. As one can see, the area covered by the hysteresis loops is reduced once the domain wall is pinned to the inclusion.

Another simulation was performed for a material with an elliptical inclusion, to mimic the precipitate shape observed in [4]. Figure 4 shows that the domain wall is again pinned to the inclusion, once it reaches it. The charge and macroscopic strain for this case are displayed in Figure 7. As the precipitate covers almost the whole travel path of the domain wall, the pinning already happens in an early stage of the simulation. This is the reason for the similar curves of the first and the second period. However, the surface covered by the hysteresis is smaller compared to the one for homogeneous material.

5 | CONCLUSION

The movement of domain walls in different ferroelectric materials was investigated by simulating the evolution of a phase field for polarization. The simulations yield the charge and strain hysteresis loops for both homogeneous material and

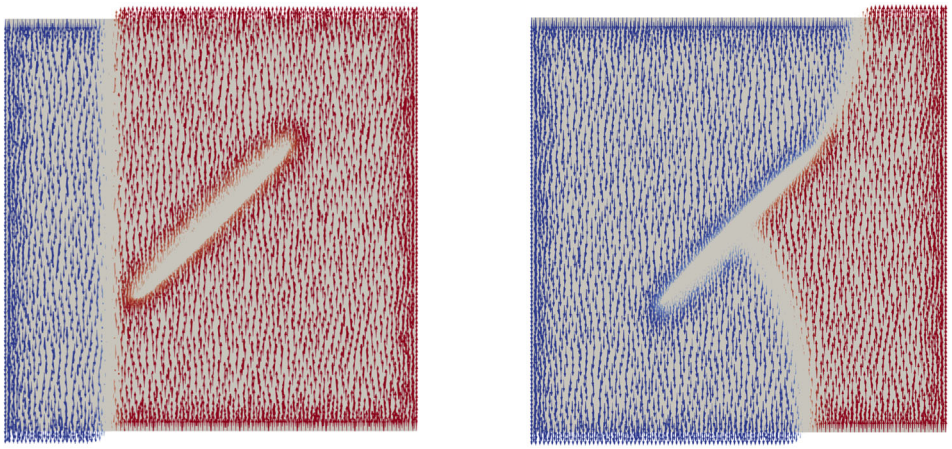

(A) (B)

FIGURE 4 Phase field with 180° domain wall for material with elliptical inclusion: (A) initial configuration and (B) pinned.

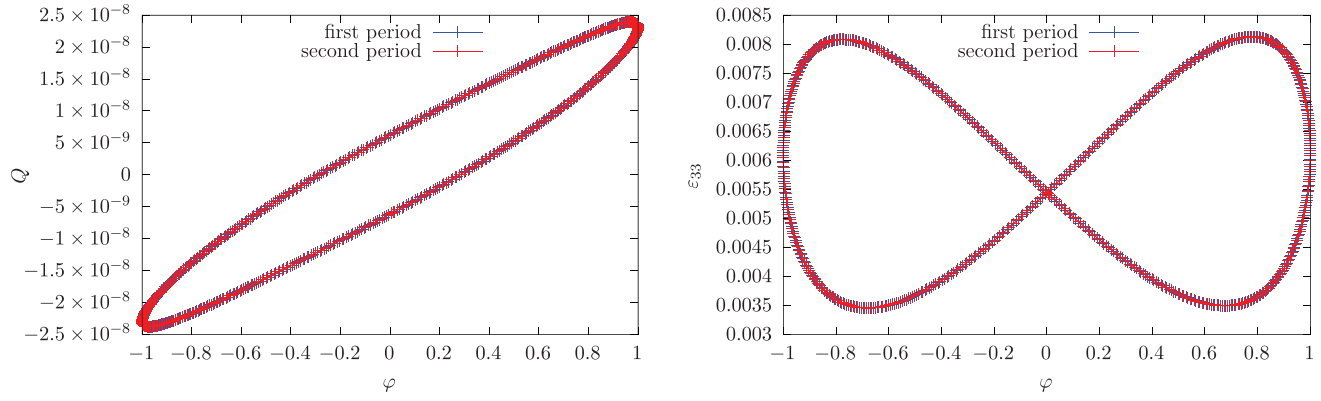

(A) (B)

FIGURE 5 Charge (A) and macroscopic strain (B) for homogeneous material.

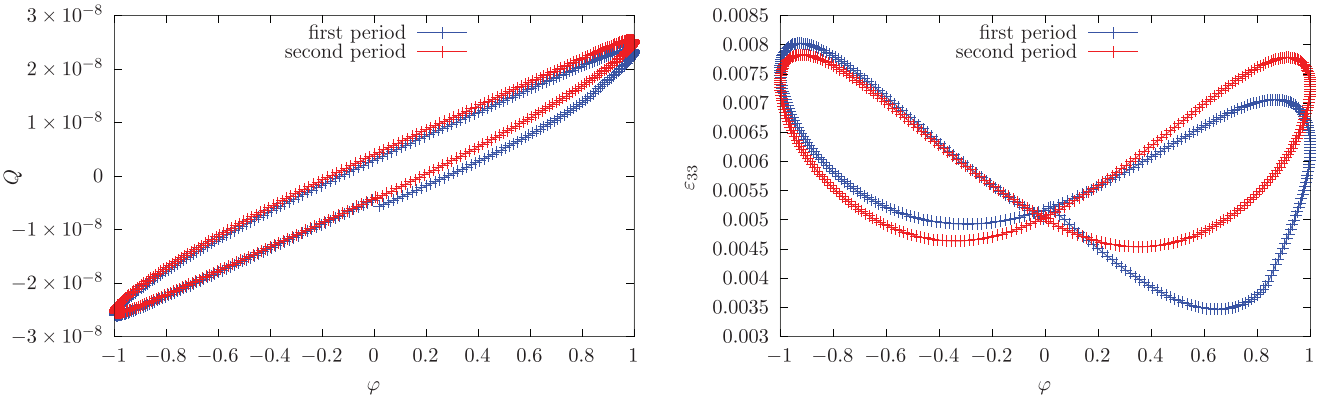

(A) (B)

FIGURE 6 Charge (A) and macroscopic strain (B) for material with circular inclusion.

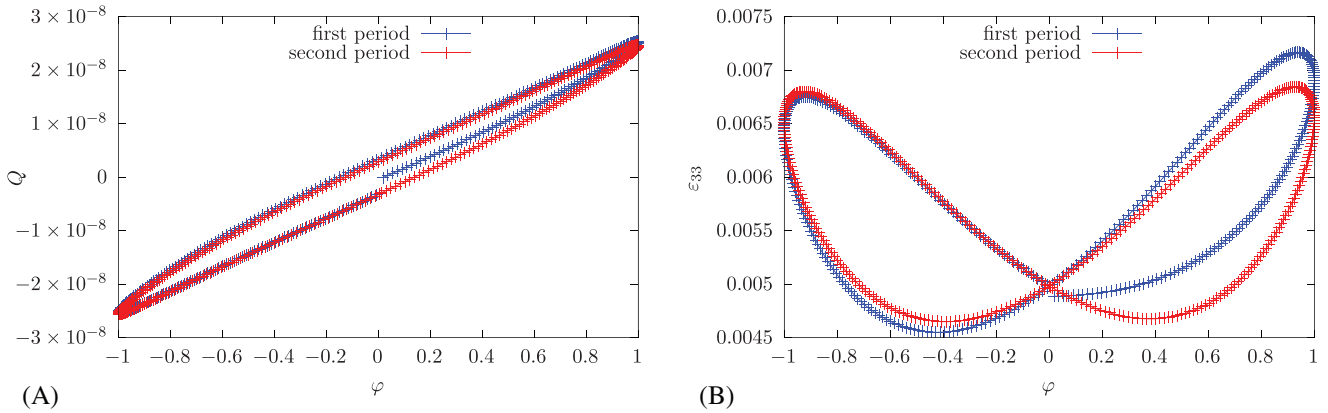

FIGURE 7 Charge (A) and macroscopic strain (B) for material with elliptical inclusion.

heterogeneous material with inclusion. As one can deduce from the presented results, the hysteresis becomes smaller when precipitates are introduced in the material. This behavior matches well with the measured curves in the recent experimental study and sets the base for further investigation on the shape and size of the precipitates, with the goal of minimizing the loss due to the hysteresis effect.

ACKNOWLEDGMENTS

Many thanks to Prof. Jürgen Rödel and his research group from the Department of Materials and Earth Sciences at TU Darmstadt for the kind exchange as well as the Lichtenberg II Cluster in Darmstadt for supporting the computations. Financial support by the DFG for the project 528293120 is appreciated.

Open access funding enabled and organized by Projekt DEAL.

ORCID

Matthias Bohnen https://orcid.org/0009-0006-5166-1337

REFERENCES

1. Lumley, R. N. (2014). Heat treatment of aluminum alloys. In R. B. Hetnarski (Ed.), *Encyclopedia of thermal stresses* (pp. 2190–2203). Springer.
2. Pollock, T., & Argon, A. (1992). Creep resistance of CMSX-3 nickel base superalloy single crystals. *Acta Metallurgica et Materialia*, *40*(1), 1–30.
3. Zhao, C., Gao, S., Yang, T., Scherer, M., Schultheiß, J., Meier, D., Tan, X., Kleebe, H., Chen, L., Koruza, J., & Rödel, J. (2021). Precipitation hardening in ferroelectric ceramics. *Advanced Materials*, *33*(36), 2102421.
4. Gao, S., Zhao, C., Bohnen, M., Müller, R., Rödel, J., & Kleebe, H. J. (2023). Precipitate-domain wall topologies in hardened Li-doped $NaNbO_3$. *Acta Materialia*, *254*, 118998.
5. Schrade, D., Mueller, R., Xu, B., & Gross, D. (2007). Domain evolution in ferroelectric materials: A continuum phase field model and finite element implementation. *Computer Methods in Applied Mechanics and Engineering*, *196*(41-44), 4365–4374.
6. Kamlah, M. (2001). Ferroelectric and ferroelastic piezoceramics – Modeling of electromechanical hysteresis phenomena. *Continuum Mechanics and Thermodynamics*, *13*(4), 219–268.
7. Alnaes, M. S., Blechta, J., Hake, J., Johansson, A., Kehlet, B., Logg, A., Richardson, C., Ring, J., Rognes, M. E., & Wells, G. N. (2015). The FEniCS project version 1.5. *Archive of Numerical Software*, *3*(100), 9–23.
8. Logg, A., Ølgaard, K. B., Rognes, M. E., & Wells, G. N. (2012). FFC: The FEniCS form compiler. In A. Logg, K. Mardal, & G. N. Wells (Eds.), *Automated solution of differential equations by the finite element method*, Lecture notes in computational science and engineering (Vol. 84, chap. 11). Springer.
9. Ding, H., & Chen, W. (Eds.). (2001). *Three dimensional problems of piezoelasticity*. Nova Science Publishers.

How to cite this article: Bohnen, M., & Müller, R. (2023). Simulation of precipitate hardening in ferroelectric material. *Proceedings in Applied Mathematics and Mechanics*, *23,* e202300215.
https://doi.org/10.1002/pamm.202300215